COMPARATIVE STUDY OF THE PARALLEL AND ANGULAR ELECTRICAL GRIPPER FOR INDUSTRIAL APPLICATIONS

Mohammad Javad FOTUHI [*], **Zafer BINGUL** [**]

[*]Research and Development, Keramik Makina Sanayi ve Ticaret A.S,
Güzeller Organize Sanayi Bölgesi İnönü Mah. Nursultan Nazarbayev Sok. No:21 41400 Gebze, Kocaeli, Turkey
[**]Automation and Robotics Lab, Department of Mechatronics Engineering, Kocaeli University,
Kabaoğlu, Baki Komsuoğlu bulvarı No:515, Umuttepe, 41001 İzmit/Kocaeli, Turkey

mohammad.fotuhi@keramik.com.tr, zaferb@kocaeli.edu.tr

Abstract: The aim of this paper is to study the position and power performances of an electrical lead screw-driven industrial gripper mechanism (LSDIGM). This work consists of designing and developing an electrical LSDIGM that has the potential to meet various demands in the automation industry and factories. The performances of both angular electrical gripper (AEG) and parallel electrical gripper (PEG) mechanisms were compared based on their position and power efficiency. The position efficiency of these electrical LSDIGM is computed from the position root mean square error (PRMSE) obtained from errors between the two measured positions (input incremental encoder and output linear encoder). In the experimental setup, a current sensor and a spring were employed to measure the current in the input of the system and the stiffness in the output of the system, respectively. The electrical power in the input of the electrical LSDIGM and the mechanical power in the output of the LSDIGMs were calculated using the current and the spring force, respectively. Finally, the power efficiency of these electrical LSDIGMs was examined and compared at different velocity circumstances.

Key words: Electrical lead screw-driven industrial gripper mechanism (LSDIGM), Efficiency, Position root mean square error (PRMSE),
Parallel electrical gripper (PEG), Angular electrical gripper (AEG)

1. INTRODUCTION

Nowadays, designing and developing an inexpensive and reliable electric gripper mechanism in factories is very important in the robotic manufacturing revolution. In robotic systems, the gripper is like the human hand that allows one to grab and place any particular object. Grippers have been used in factories to facilitate various operations and for tasks that are dangerous and difficult for humans to perform, such as logistics, underwater welding, material handling, sensitive surgery, detecting and defusing bombs, and industrial furnaces (Birglen and Schlicht, 2018). The basic requirements of the gripper system design should be characterized as follows: high power/weight ratio giving the lowest machine mass, high torque/inertia ratio giving the best acceleration possible, the smooth trajectory of torque particularly at low speeds to minimize speed variation and achieve good positional accuracy, controlled torque at zero-speed, high maximum speed of operation, high efficiency and power factor to minimize drive requirement, compact integrated design with the application, good frequency response, low backlash, and low cost (Liu et al, 2020). To develop an industry interesting product, there is a need for inexpensive, simple, and robust solutions. Industrial robotic grippers have an effective role in modern automation as they constitute the end-of-arm of robotic manipulators and then, they are in direct contact with the work piece (Honarpardaz et al, 2017; Lu et al., 2019). Also, with the development of series elastic actuators and control methods, flexible grippers can be developed; flexible grippers have more accuracy of control and gripping force (Li et

al., 2017). With the advent of modeling and simulation technology, design and development studies are increasingly focusing on robotics research. The key challenge in these problems is to find the right balance between all the conflicting goals. The perfect solution to an optimal design problem of a given gripper system is to develop a set of solutions by analyzing the system parameters that accomplish all the goals simultaneously (Kuang et al., 2017; Hu et al, 2019).

In a variety of industrial applications, hydraulic and pneumatic grippers are used to create a holding force according to specific specifications, depending on the load. However, hydraulic and pneumatic methods are not flexible and cannot be used in the manufacture of modern systems (Kumar et al., 2017). Today, a mechanical gripper in the system and mechatronics engineering are increasingly being replaced by electrically controlled drives called the electrical actuator (Tai et al., 2016). The electrical gripper is a mechanism used to perform linear motion electrically similar to that achieved with hydraulic and pneumatic grippers. In the main component of the electrical gripper, the classical mechanical gripper is replaced with an electrical motor and reprogrammable controller. Compared to the mechanical grippers, the electrical gripper improves accuracy and repeatability (Shin et al., 2012). The servomotors used in modern electrical grippers are well suited for complex motions because they are easy to control by changing the voltage and current, speed, and torque in the servomotors. However, motion systems using the feedback feature in these motors are expensive and quite complex. This is one of the main reasons why a stepper motor is used as an actuator

in a proposed electronic gripper system while considering the low price and easy usage (Datta et al., 2015). A stepper motor is a motor that converts digital electric pulses into stepping mechanical movements. The most important advantage of a stepper motor is its use in an accurately open-loop control system. This type of control eliminates the need for expensive detection and feedback devices such as sensitive encoders. Its position is simply determined by tracking the input electrical pulses (Shaw and Dubey, 2016). The stepper motor can be a good selection for open-loop motion control. Stepper motors can be used in projects where rotation angle, speed, position, and synchronization must be controlled. Stepper motors can be used in many different projects (Su and Zhong, 2018). Because of these main advantages, a stepper motor is selected as an actuator for electromechanical gripper movement output in this paper. In this paper, the application of the lead screw-driven industrial gripper mechanism (LSDIGM) was developed from the switching of the existing pneumatic cylinder. The main goal of such a system is to avoid force overshoots in the contact stage while keeping stress force error in the high-sensitive tracking stage, where traditional pneumatic cylinders are not competent. The proposed method of the ratio of the maximum force (RMF) has been used to prove the appropriate force rate. In this study, the lead screw and electrical motor-driven industrial gripper mechanism model was developed to have a flexible and reprogrammable system. First, the design and modeling of electrical LSDIGM are briefly introduced. Then, the overall behavior structure of the system is proposed. The position and power efficiency of these electrical LSDIGMs were examined and compared at different velocity circumstances.

2. MATERIALS AND METHODS

In the case of rotational actuators, first, the movement forms have to be converted from rotational to linear movement. This can be achieved by a connecting lead screw to the actuator and a linear guide the diagram of the electrical LSDIGM is illustrated in Fig.1. For the electrical gripper, a model was developed in Li et al. (2011) and Chen et al. (2014). The mathematical model is based on two movements: the movement angle, θ, to the motor angle and the movement distance to the load movement. The θ angle is linked by a lead-screw mechanism to the *d* distance. The resultant angular motion and linear motion produce two respective forces: a lead-screw torsional torque τ_{ls} applied at the input of the system and a gripper linear force F_g applied at the output of the system.
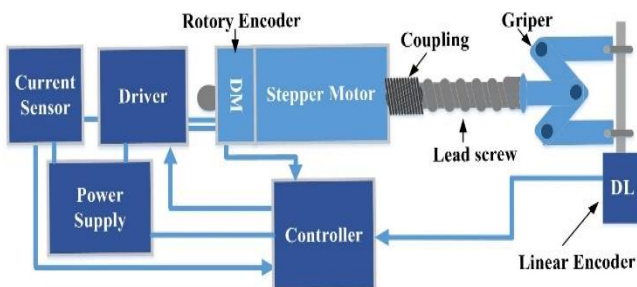

Fig. 1. Block diagram of the LSDIGM

In order to evaluate the performance of position errors, in general, the square root of the mean of all square errors (PRMSE) is calculated between the stepper motor position and the meas-

ured load signal based on equation 1 (Chen et al., 2014; Nanda, 2010). The equations (2, 3, 4, 5) are used to illustrate the effect of time and position error in equation 1.

$$PRMSE = \sqrt{\frac{1}{N}\sum_{i=1}^{N}(p_i - \hat{p}_i)^2} \tag{1}$$

Integral of the absolute value of the error (IAE):

$$IAE = \sum_{i=1}^{N}|(p_i - \hat{p}_i)| \tag{2}$$

Integral of the square value of the error (ISE):

$$ISE = \sum_{i=1}^{N}(p_i - \hat{p}_i)^2 \tag{3}$$

Integral of the time-weighted absolute value of the error (ITAE):

$$ITAE = \sum_{i=1}^{N}t|(p_i - \hat{p}_i)| \tag{4}$$

Integral of the time-weighted square value of the error (ITSE):

$$ITSE = \sum_{i=1}^{N}t(p_i - \hat{p}_i)^2 \tag{5}$$

where p_i is the output position, $\hat{p}_i$ is the input position, *t* is the sampling time, and *N* is the sampling number (Najjari et al., 2014).

In this paper, a standard algorithm using a C++ programming language is implemented in a Googoltech industrial PC to run the LSDIGM system. The stepper motor can be programmed and controlled in real-time by using this software via the output port of an industrial PC. In order to perform the gripper movement, the proposed method uses a lead screw for converting the rotary movement of the stepper motor into the linear movement.

2.1. Mechanical Design

To obtain a simple and inexpensive design, we minimized the amount of mechanical and electronic parts (Fig. 2). It was, therefore, decided to use a normal stepper motor and lead screw. Also, angular gripper and parallel gripper can be both opened and closed by only one HANPOSE 17HS3401S T8x8 Nema stepper motor with a PK6M05N lead screw driven by the stepper motor driver model CWD556 (Fig. 3). When a voltage of 24 V is applied to the motor, this results in a constant actuation torque of 0.5 Nm applied at the base of the finger and 0.25 Nm on each of the opposite fingers as defined (Park et al., 2016). First, it is required to determine the torque of the motor relative to the system's output force, the torque due to the force the load applies to the gripper finger called gripper force F_g(N), and it is introduced through function F_g. The gripper force is given in equation (6) as mentioned before; for rotational actuators, the movement has to be converted from rotational to linear. To calculate the velocity of the motor, the linear speed of the gripper finger can be converted to rotational speed using equation (7).

$$F_g = \frac{2\pi\,\eta\,\tau_{ls}}{\ell} \tag{6}$$

$$v = \frac{\ell\omega}{2\pi} \tag{7}$$

where F_g is the force/load applied (N), η is the efficiency factor, ω is the rotational speed (rad/sec), and *v* is the linear speed (mm/sec) (Liu et al., 2016). Torque τ_{ls} is the lead-screw acting on the shaft caused by forces (see Fig. 4). It can be based on the following equations (8):

Mohammad Javad Fotuhi, Zafer Bingul
Comparative Study of the Parallel and Angular Electrical Gripper for Industrial Applications

DOI 10.2478/ama-2021-0010

$$\tau_{ls} = \frac{F_a D_x}{2}\left(\frac{\ell + \mu\pi D_x}{\pi D_x - \mu L}\right)\left(\frac{1}{\eta}\right) \tag{8}$$

where:

$$D_x = D_p - \left(\frac{P_B}{2}\right), \quad \ell = n_s P_B \tag{9}$$

F_a is the moving force in the direction of the lead screw, and θ is the tilt angle (Xu et al., 2018; Hassan and Abomoharam, 2017). The parameters of the lead-screw model are given in Table 1.
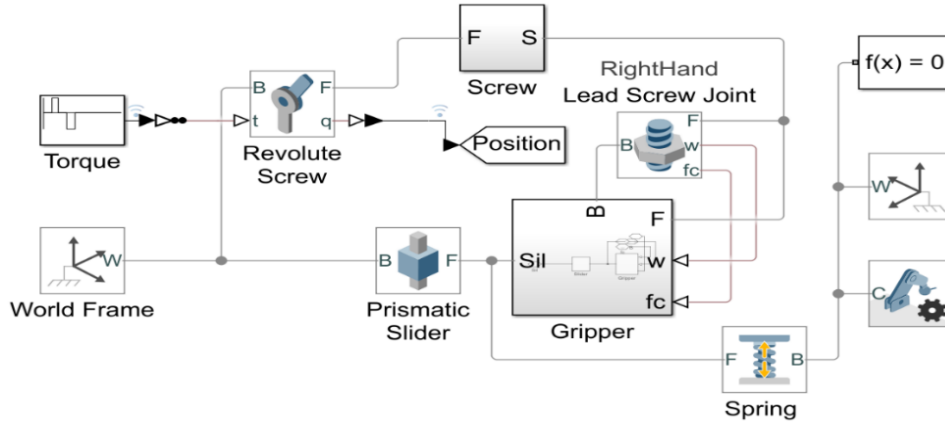

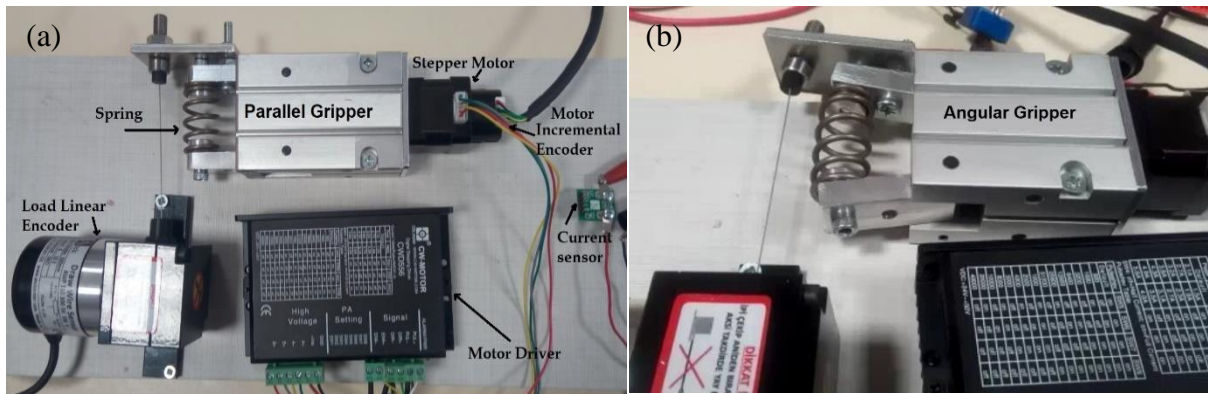**Fig. 2**. Simscape model of the electrical LSDIGM actuator

Fig. 3. Experimental setup of LSDIGM (a) parallel gripper and (b) angular gripper
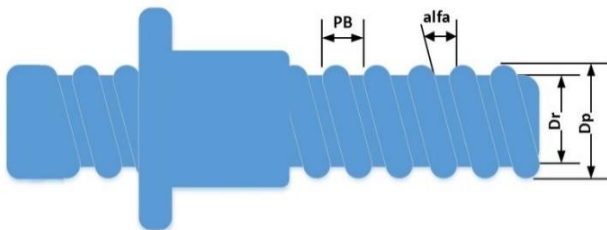

Fig. 4. Model of the lead screw

Tab. 1. Parameters of lead-screw model-PK6M05N

Parameter	Symbol	Value
Pitch circle diameter	D_p	9.5 mm
Screw pitch	P_B	5 mm
Lead of the thread	ℓ	5 mm
The starts number	n_s	1
Friction coefficient of sliding surface	μ	0.15
Thread angle	A	30 degree

2.2. Modeling of Electromechanical System

To analyze the dynamic characteristics after the completion of the development of the electromechanical system, an electrical LSDIGM actuator model was created in SIMULINK™ (Fig. 2).

Contributions from the different system variables were combined to simplify the model. The motor rotor inertia, screw nut inertia, and carrier inertia were combined, along with the referred inertial contribution from the linear motion parts and were represented by equation (10).

$$J_{tot} = J_{motor} + J_{nut} + J_{carrier} + m\left(\frac{L}{2\pi}\right)^2 \tag{10}$$

where *m* is the mass of the linear components, and ℓ is the screw lead. This leads to

$$J_{tot}\alpha = \tau_{motor} - (\tau_{load} + \tau_{viscous} + \tau_{Coulomb}) \tag{11}$$

$$J_{tot}\frac{d^2\theta}{dt^2} = \tau_{motor} - \left(F_g X + \beta\frac{d\theta}{dt} - F_c\frac{\frac{d\theta}{dt}}{\left|\frac{d\theta}{dt}\right|}\right) \tag{12}$$

where F_g is the force on the gripper fingers, *j* represents the gear ratio and linear conversion, β represents the viscous damping coefficient, and *F*c represents the Coulomb force component.
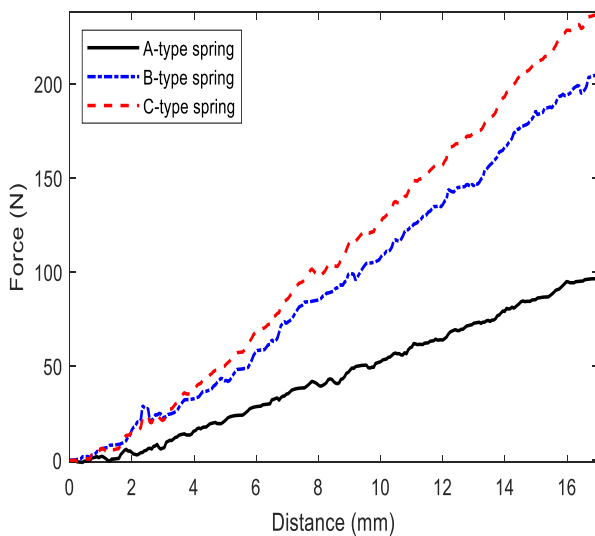

Fig. 5. Force–distance (stiffness) characteristic of the springs given in Table 3

3. RESULTS AND DISCUSSION

There are several methods for analyzing and measuring force, three springs with different stiffness coefficient values (Fig. 5 and Table 3) have been used to analyze the dynamic behavior of the system (Fotuhi et al., 2020). To analyze the gripper, two sensors were used to measure data. Sensors are incremental encoders of motor and linear encoders of load (Fotuhi and Bingul, 2021; Wang et al., 2016). Motor incremental encoder gives a pulse output of 0.17578125 (degrees/pulse), and load linear encoder gives a voltage output of 0.5 (mV/mm). Over the range 0–20 mm, this is amplified by an amplifier with a voltage gain of 20, sampled, and applied to a 10-bit analog-to-digital converter with voltage range 0–5 V. The resolution of the measurement is 1024 (digital value/mm). The experimental setup of electrical LSDIGM is shown in Fig. 3. The position and current analog signals are converted to physical parameters by using sensor gains (equations 13, 14, and 15). They are given in Table 2.

$$D_L(mm) = (V_L - o_v) * (c_V) \qquad (13)$$

$$D_M(mm) = (P_M - o_p) * (c_P{}^{-1}) \qquad (14)$$

$$C_s(Amper) = (V_c - o_c) * (c_c{}^{-1}) \qquad (15)$$

here, D_L is the distance of load (mm), D_M is the distance of linear movement of motor (mm), C_s is the equation of current sensing, V_L is the digitized voltage from analog to digital using an ADC (analog-to-digital converter) value of voltage output of the load linear encoder (digital value), P_M is the pulse number of the motor incremental encoder (pulse), and V_c is the discrete voltage (ADC value of voltage) output of the current sensor.

Tab. 2. Position and current sensor gains

Parameter	Symbol	Value
Voltage coefficient of the linear encoder	c_V	1.427428571
Pulse coefficient of the incremental encoder	c_P	1.0058
Current coefficient of the current sensor	c_c	29.457
Offset of voltage	o_v	779.7638571
Offset of pulse	o_p	62.41924891
Offset of current	o_c	17.92554531

Tab. 3. Technical specification of springs

Spring type	Stiffness (*Ks* = N/mm)	Free length (mm)	Full compression (mm)	Total coil
A	5.735	42.1	25.3	7
B	11.764	42.5	25.2	7
C	13.823	42.2	25.6	7

Tab. 4. Velocity profile (maximum speed = 30 mm/sec)

Speed mode	Speed	Speed (mm/sec)
Low speed (LS)	5% Max	1.5
Medium speed (MS)	20% Max	6
High speed (HS)	65% Max	19.5
Very high speed (VHS)	85% Max	25.5

To avoid repetition of showing the same behavior in the paper, the movement profile of a parallel and angular gripper A-type of the spring in the low-speed case is only illustrated in Fig. 6. The results of the medium, high, and very high speed of B-type and C-type of springs for parallel and angular gripper are given also in Tables 5 and 6. The velocity profile is shown in Table 4.

According to Table 5, for the A-type spring, the maximal force of 106.4 N and the maximum linear movement of 18.55 mm are obtained by the high velocity of 5.892 mm/sec. For the B-type spring, the maximal force of 100 N and the maximum linear movement of 9 mm are obtained by the high velocity of 1.375 mm/sec. For the C-type spring, the maximal force of 105 N and the maximum linear movement of 8.013 mm are obtained by the high velocity of 1.375 mm/sec. According to Table 6, for the A-type spring, the maximal force of 65.36 N and the maximum linear movement of 11.55 mm are obtained by the high velocity of 1.378 mm/sec. For the B-type spring, the maximal force of 84.86 N and the maximum linear movement of 6.966 mm are obtained by the high velocity of 1.375 mm/sec. For the C-type spring, the maximal force of 103.7 N and the maximum linear movement of 7.504 mm are obtained by the high velocity of 1.371 mm/sec.

According to Table 7, equations (2, 3, 4, and 5) are used to illustrate the effect of time and position error in equation (1).
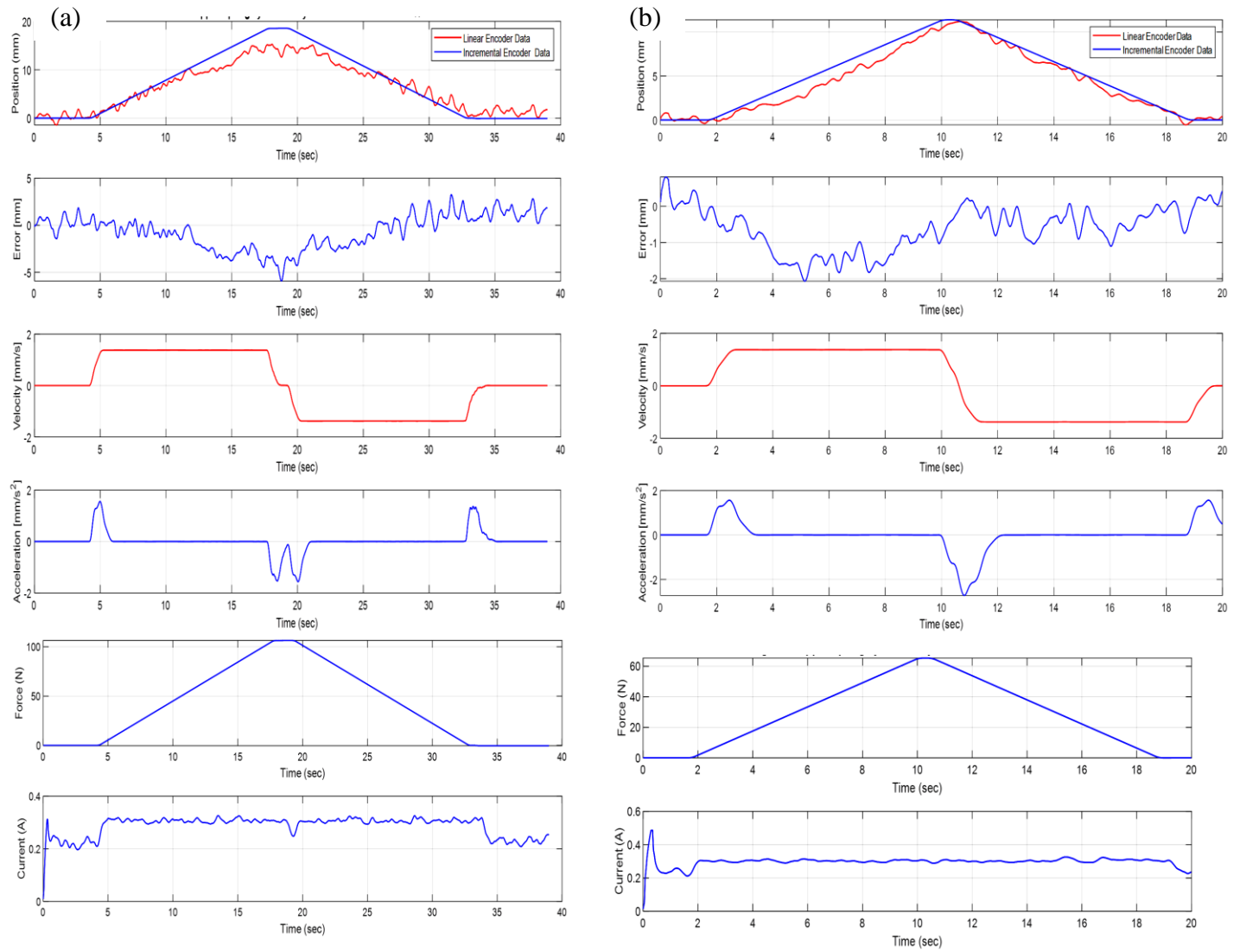
Fig. 6. The motion profile of a (a) parallel gripper and (b) angular gripper A-type spring in the LS mode

Tab. 5. Parallel gripper and spring motion analysis

Spring type	Speed mode	Maximum linear movement (mm)	Maximum force (N)	Time (sec)	Maximum current (A)	Maximum velocity (mm/sec)	Maximum acceleration (mm/sec²)
A	LS	18.54	106.4	28.869	0.3155	1.376	1.547
	MS	18.51	106.3	8.79	0.3150	5.892	6.598
	HS	17.26	103.73	3.735	0.3399	18.88	22.24
	VHS	6.085	34.9	4.26	0.3106	9.991	19.75
B	LS	9.09	106	13.49	0.7168	1.375	1.523
	MS	8.934	105.1	9.675	0.3161	5.889	6.336
	HS	8.934	105.1	4.59	0.3228	12.34	18.22
	VHS	2.827	33.26	6.21	0.3088	5.179	9.689
C	LS	8.013	105	14.45	0.3129	1.376	1.553
	MS	8.0	104	7.755	0.3045	5.887	6.667
	HS	7.864	101.1	3.38	0.3203	11.12	17.82
	VHS	1.935	25.39	69.08	0.2786	3.25	4.675

Tab. 6. Angular gripper and spring motion analysis

| Spring type	Speed mode	Maximum linear movement (mm)	Maximum force (N)	Time (sec)	Maximum current (A)	Maximum velocity (mm/sec)	Maximum acceleration (mm/sec²)
A	LS	11.4	65.36	17.525	0.4862	1.378	1.561
	MS	11.4	65.36	8.04	0.3203	5.887	6.682
	HS	7.28	55.1	4.275	0.3176	11.74	17.94
	VHS	5.047	28.94	2.565	0.2941	8.848	16.75
B	LS	6.966	84.86	14.355	0.3765	1.375	1.528
	MS	6.611	79.27	3.51	0.3105	5.883	7.712
	HS	6.362	74.84	2.37	0.322	9.028	15.96
	VHS	4.137	48.67	44.087	0.3099	13.24	53.43
C	LS	7.504	103.7	20.7	0.3033	1.371	1.495
	MS	7.144	101.7	5.13	0.3094	5.886	6.586
	HS	6.847	98.21	3.386	0.3081	10.763	17.16
	VHS	3.714	51.32	2.40	0.3071	6.264	11.45
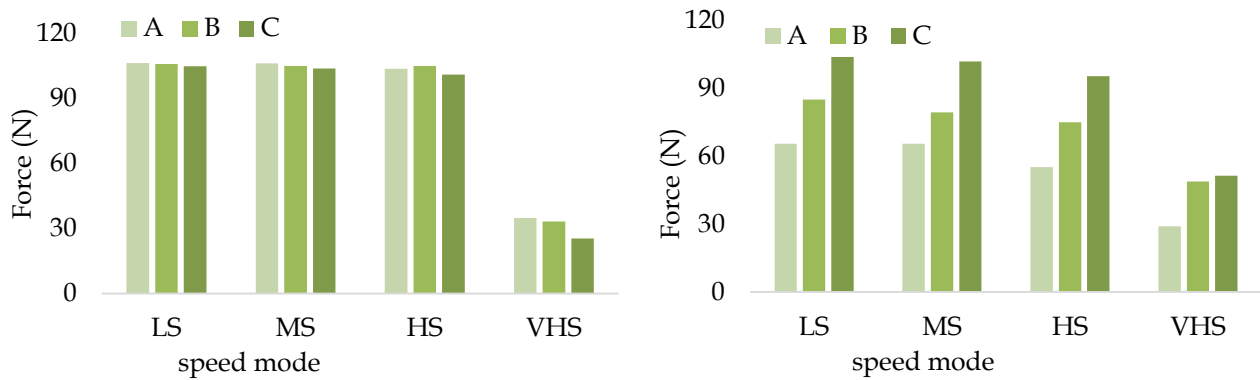
Fig. 7. (a) Parallel and (b) angular gripper spring force analysis. Note: A-type, B-type, and C-type spring

Tab. 7. RMS position error (ISE method) comparison of different speed cases (unit: mm). Note: A-type, B-type and C-type spring

Speed mode	Parallel gripper			Angular gripper		
	A	B	C	A	B	C
LS	0.0113	0.0199	0.0110	0.0557	0.0350	0.0117
MS	0.0146	0.0323	0.0151	0.0784	0.0554	0.0354
HS	0.0266	0.0379	0.0273	0.1177	0.0847	0.0473
VHS	0.0260	0.0140	0.0085	0.0280	0.3765	0.0610

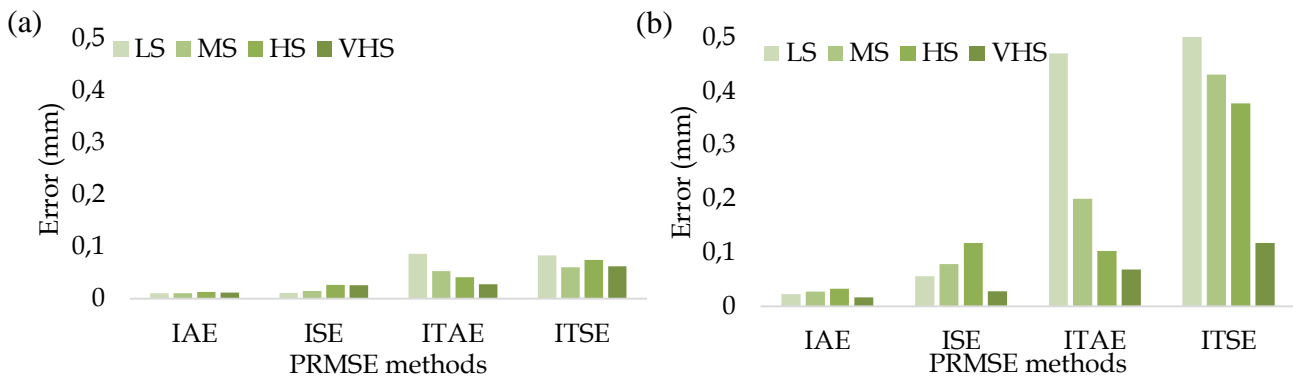**Fig. 8**. The PRMSEs of different speed cases with A-type spring: (a) parallel gripper and (b) angular gripper

Mohammad Javad Fotuhi, Zafer Bingul
Comparative Study of the Parallel and Angular Electrical Gripper for Industrial Applications

DOI 10.2478/ama-2021-0010

To evaluate the performance of the maximum force of the electrical LSDIGM, the ratio of the maximum force (RMF) between the desirable force (F_d) and the measured force (F_m) of the system is calculated based on the following equation (16) (Varanasi and Nayfeh, 2004). These ratios are given in Tables 8 and 9. The RMF is the highest ratio of the force applied by the system to the spring.

$$\text{RMF} = \left(1 - \left(\frac{F_d - F_m}{F_d}\right)\right) * 100 \qquad (16)$$

Tab. 8. The highest ratio of the force applied-PEG

Speed mode	Spring type		
	A	B	C
LS	92.52	92.17	92.45
MS	92.43	91.39	92.27
HS	90.20	91.39	86.55
VHS	30.35	44.25	46.65

The highest ratio of the force applied by the system to the A-type spring is 92.52% obtained by the low velocity of 1.376 mm/s. It can be seen that in Table 8 the lowest values are related to the fourth row of speeds (VHS) that are less than 50% and the values are unacceptable, indicating that the system did not respond correctly at this speed (Heilala et al., 1992; Pham and Yeo, 1991).

Tab. 9. The highest ratio of the force applied-AEG

Speed mode	Spring type		
	A	B	C
LS	59.42	77.15	91.30
MS	59.42	72.06	90.43
HS	50.09	68.04	87.91
VHS	26.31	28.92	22.07

The highest ratio of the force applied by the system to the C-type spring is 92.45% obtained by the low velocities of 1.495 mm/s. It can be seen that in Table 9 the lowest values are related to the fourth row of speeds (VHS) that are less than 50% and the values are unacceptable, indicating that the system did not respond correctly at this speed. According to Tables 4 and 5, and applying speeds from Tables 8 and 9, the highest power for the parallel gripper is 1.96 watt (A- HS) and for the angular gripper is 1.06 watt (C- HS), respectively.
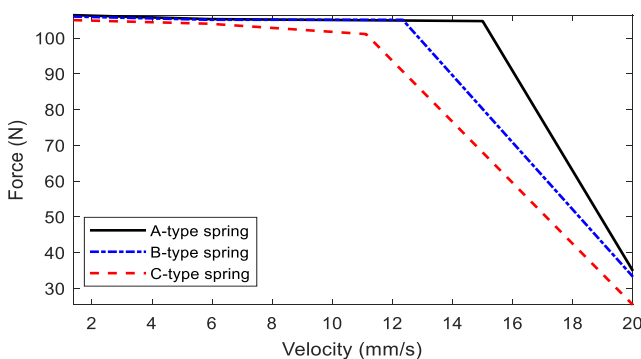

Fig. 9. Velocity–force characteristics

For three springs with different stiffness coefficient values, the force analysis of two different grippers (parallel and angular) is illustrated in Fig. 7. Fig. 8 shows comparison of the position error of the grippers with A-type spring in different speed cases. As can be seen in Fig. 9 (taken from the data in Table 5), the output force of the parallel gripper is nearly constant with 105 N at the velocities of between 1.5 and 12 mm/sec. This relationship between force and speed can be seen in Figs. 7, 8 and 9. The best angular gripper efficiency with a spring stiffness of 11.764 at a velocity of 1.5 mm/sec, which is 29%, and the best parallel gripper efficiency with a spring stiffness of 5.735 at a velocity of 1.5 mm/s, which is 52%.

4. CONCLUSION

In this paper, design and force–velocity performance analysis of the electrical gripper mechanism were examined. In this work, a stepper motor and a lead-screw mechanism were used for an inexpensive gripper as an industrial product. In order to test the performance of the system, an analysis of the LSDIGM, experimental setup with springs and encoders were arranged. The performance of the grippers is dependent on position and power efficiency. The LSDIGMs were tested with different springs and velocity profiles to obtain these efficiencies. The results show that the electrical parallel gripper performed better than the electrical angular gripper, and the highest ratio of the force applied by the proposed parallel gripper is 92.52% at 1.376 mm/sec. Although the proposed method has a very small (low) position error (accuracy) due to the operating characteristics of the stepper motor, it is simpler and less expensive than its counterparts. Therefore, it may be preferred for some applications where minor position errors are not important. Using the proper stepper motor (high power and high position accuracy) and the lead screw, these position errors occurred here may be eliminated very easily.

REFERENCES

1. **Birglen L., Schlicht, T.** (2018), A statistical review of industrial robotic grippers. , *Robotics and Computer-Integrated Manufacturing*, 49, 88-97.
2. **Chen Z., Xu J., Yu L., Xiong Y., Zhu H.** (2014, May), Design and implementation of the electric gripper control system based on the DSP. In *The 26th Chinese Control and Decision Conference (2014 CCDC)*, (pp. 3513-3517,). IEEE.
3. **Datta R., Pradhan S., Bhattacharya B.** (2015), Analysis and design optimization of a robotic gripper using multiobjective genetic algorithm. , *IEEE Transactions on Systems, Man, and Cybernetics: Systems*, 46(1), 16-26.
4. **Fotuhi M. J., Bingul Z.** (2021), Fuzzy torque trajectory control of a rotary series elastic actuator with nonlinear friction compensation. , *ISA transactions*.
5. **Fotuhi M. J., & Bingul Z.** (2021), Novel fractional hybrid impedance control of series elastic muscle-tendon actuator. , *Industrial Robot: the international journal of robotics research and application*.
6. **Fotuhi M. J., Yılmaz O., Bingul Z.** (2020), Human postural ankle torque control model during standing posture with a series elastic muscle-tendon actuator. , *SN Applied Sciences*, 2(2), 1-8.
7. **Hassan A., Abomoharam M.** (2017), Modeling and design optimization of a robot gripper mechanism. , *Robotics and Computer-Integrated Manufacturing*, 46, 94-103.
8. **Heilala J., Ropponen T., & Airila M.** (1992), Mechatronic design for industrial grippers. , *Mechatronics*, 2(3), 239-255.

9. **Honarpardaz M., Tarkian M., Ölvander J., Feng X.** (2017), Finger design automation for industrial robot grippers: A review. , *Robotics and Autonomous Systems*, *87*, 104-119.

10. **Hu Z., Wan W., Harada K.** (2019), Designing a mechanical tool for robots with two-finger parallel grippers. , *IEEE Robotics and Automation Letters*, *4*(3), 2981-2988.

11. **Kuang L., Lou Y., Song S.** (2017), Design and fabrication of a novel force sensor for robot grippers. , *IEEE Sensors Journal*, *18*(4), 1410-1418.

12. **Kumar R., Mehta U., Chand P.** (2017), A low cost linear force feedback control system for a two-fingered parallel configuration gripper. , *Procedia computer science*, *105*, 264-269.

13. **Li Q. M., Qin Q. H., Zhang S. W., Deng H.** (2011), Optimal design for heavy forging robot grippers. , In *Applied Mechanics and Materials* (Vol. , 44, pp. 743-747). , Trans Tech Publications Ltd.

14. **Li X., Chen W., Lin W., Low K. H.** (2017), A variable stiffness robotic gripper based on structure-controlled principle. , *IEEE Transactions on Automation Science and Engineering*, *15*(3), 1104-1113.

15. **Liu C. H., Chung F. M., Chen Y., Chiu C. H., Chen T. L.** (2020), Optimal Design of a Motor-Driven Three-Finger Soft Robotic Gripper. , *IEEE/ASME Transactions on Mechatronics*, *25*(4), 1830-1840.

16. **Liu Y., Zhang Y., Xu Q.** (2016), Design and control of a novel compliant constant-force gripper based on buckled fixed-guided beams. , *IEEE/ASME Transactions on Mechatronics*, *22*(1), 476-486.

17. **Lu, Y., Xie , Z., Wang, J., Yue, H., Wu, M., & Liu, Y.** (2019), A novel design of a parallel gripper actuated by a large-stroke shape memory alloy actuator. , *International Journal of Mechanical Sciences*, *159*, 74-80.

18. **Najjari B., Barakati S. M., Mohammadi A., Futohi M. J., Bostanian M.** (2014), Position control of an electro-pneumatic system based on PWM technique and FLC. , *ISA transactions*, *53*(2), 647-657.

19. **Nanda A. P.** (2010), *Design & Development of a Two-jaw parallel Pneumatic Gripper for Robotic Manipulation* (Doctoral dissertation).

20. **Park T. M., Won S. Y., Lee S. R., Sziebig G.** (2016, June), Force feedback based gripper control on a robotic arm. In, *2016 IEEE 20th Jubilee International Conference on Intelligent Engineering Systems (INES),* (pp. 107-112,). IEEE.

21. **Pham D. T., Yeo S. H.** (1991), Strategies for gripper design and selection in robotic assembly. , *The International Journal of Production Research*, *29*(2), 303-316.

22. **Shaw J. S., Dubey V.** (2016, August), Design of servo actuated robotic gripper using force control for range of objects. , In *2016 International Conference on Advanced Robotics and Intelligent Systems (ARIS)* (pp. 1-6).), IEEE.

23. **Shin D. H., Park T. S., Jeong C. P., Kim Y. G., An J. N**. (2012), Study of torsion spring's parameters with angular type grippers. , In *Advanced Materials Research* (Vol. , 502, pp. 355-359). .Trans Tech Publications Ltd.

24. **Su K. H., Zhong Y. H.** (2018, July), Design of Handling Gripper and its Application to Smart Pet Robot. , In *2018 International Conference on Machine Learning and Cybernetics (ICMLC)* (Vol. , 1, pp. 105-108). IEEE..

25. **Tai K., El-Sayed A. R., Shahriari M., Biglarbegian M., Mahmud S.** (2016), State of the art robotic grippers and applications. , *Robotics*, *5*(2), 11.

26. **Varanasi K. K., & Nayfeh S. A.** (2004), The dynamics of lead-screw drives: low-order modeling and experiments. , *J. Dyn. Sys., Meas., Control*, *126*(2), 388-396.

27. **Wang X., Xiao Y., Fan X., & Zhao Y.** (2016, May), Design and grip force control of dual-motor drive electric gripper with parallel fingers. , In *2016 IEEE Information Technology, Networking, Electronic and Automation Control Conference*, (pp. 696-700,). IEEE.

28. **Xu F., Wang B., Shen J., Hu J., Jiang G.** (2018), Design and realization of the claw gripper system of a climbing robot. , *Journal of Intelligent & Robotic Systems*, *89*(3), 301-317.